

Compressibility of graphene

D. S. L. Abergel, E. H. Hwang, and S. Das Sarma

Condensed Matter Theory Center, Department of Physics, University of Maryland, College Park, Maryland 20742, USA

(Received 8 November 2010; published 28 February 2011)

We develop a theory for the compressibility and quantum capacitance of disordered monolayer and bilayer graphene, including the full hyperbolic band structure and band gap in the latter case. We include the effects of disorder in our theory, which are of particular importance at the carrier densities near the Dirac point. We account for this disorder statistically using two different averaging procedures: first via averaging over the density of carriers directly, and then via averaging in the density of states to produce an effective density of carriers. We also compare the results of these two models with experimental data, and to do this we introduce a model for interlayer screening which predicts the size of the band gap between the low-energy conduction and valence bands for arbitrary gate potentials applied to both layers of bilayer graphene. We find that both models for disorder give qualitatively correct results for gapless systems, but when there is a band gap in the low-energy band structure, the density of states averaging is incorrect and disagrees with the experimental data.

DOI: [10.1103/PhysRevB.83.085429](https://doi.org/10.1103/PhysRevB.83.085429)

PACS number(s): 73.22.Pr, 71.23.-k

I. INTRODUCTION

Recently, graphene has become a highly studied electronic system with many potential uses in electronic devices, optics, and sensing applications.¹ While significant theoretical effort has been concentrated on the transport properties² (such as the minimal conductivity, localization effects, and signatures of relativistic behavior of the charge carriers), bulk thermodynamic quantities such as the compressibility of the electron liquid in monolayer and bilayer graphene have also received substantial attention. The compressibility is an important quantity because it is possible to extract information about the electron-electron interactions and correlations directly from these measurements, and to gain information about fundamental physical quantities such as the pair-correlation function. The quantum capacitance^{3,4} is also an important quantity in the context of device design and fundamental understanding of the graphene system. In fact, the compressibility is often inferred from the measurement of quantum capacitance.

Experiments⁵ have shown that the contribution to the compressibility of monolayer graphene from electron-electron interactions is small (amounting to a 10%–15% renormalization of the effective Fermi velocity). This was explained within the Hartree-Fock approximation.⁶ Capacitance measurements of bilayer graphene have also been carried out recently,^{7,8} and they purport to show data that indicates that the quadratic approximation of the band structure of this material does not produce the correct predictions for the quantum capacitance of the graphene sheet. Other measurements that claim to access the quantum capacitance directly have shown similar behavior.⁹

Theoretical work has been published that considers the compressibility of monolayer⁶ and bilayer¹⁰ graphene at the Hartree-Fock level and in the random-phase approximation¹¹ (RPA). They find that interactions are more important in the bilayer system (owing to the finite density of states at charge neutrality), but that in the RPA the contributions from exchange and correlation almost cancel each other out, leaving a small positive compressibility at all densities. A consensus has developed that many-body corrections to the compressibility

in graphene are at most of the order of 10% at reasonable carrier densities.¹²

In this article we discuss theoretically the compressibility of monolayer and bilayer graphene, and specifically employ the four-band model of bilayer graphene (which generates the nonquadratic band structure). We will highlight the similarities and differences between this model and the linear and quadratic cases, and take into account the possibility of a gap at the charge-neutrality point. We find that the nonquadratic band structure significantly affects the theoretical predictions for the compressibility and brings them into qualitative and semiquantitative agreement with experimental findings. We also include disorder in the form of electron-hole puddles created by charged impurities in the vicinity of the graphene. We discuss two different procedures for including this effect statistically and determine the validity of each model by comparing with experimental data. The first assumes that the disorder creates a spatial variation in the density of carriers that can be modeled by averaging a physical quantity such as compressibility over a range of densities. The second model assumes that disorder affects the local density of states that can be averaged to give an effective bulk density of carriers that can then be used to compute the physical quantities of interest. We find that for gapless graphenes, inclusion of disorder by either method predicts qualitatively correct results in agreement with experiments, but when a gap is opened, the stage at which the averaging is done makes a critical difference.

Therefore, we have dual complementary theoretical goals in this work. Our primary goal is to develop an accurate (and essentially approximation-free) theory for the graphene compressibility within the noninteracting electron model that incorporates all aspects of the realistic band structure as well as effects of the disorder within reasonable and physically motivated approximations. Our secondary goal is to compare our theory closely and transparently with the existing experimental data on the compressibility of bilayer graphene so as to obtain some well-informed conclusions about the possible role of many-body exchange-correlation effects, which have recently been studied the literature^{10–12} but which are beyond the scope of the current work. We believe that an accurate calculation

of graphene compressibility within the free-electron theory neglecting all interaction effects is warranted for (at least) three reasons: (i) Without an accurate one-electron theory, quantitative conclusions regarding many-body effects are not useful; (ii) many-body theory is, by definition, approximate and, as such, subject to doubt; and (iii) many-body corrections to graphene compressibility are claimed to be small with considerable cancellation between exchange and correlation effects.¹¹ In comparing our theoretical results with the experimental data, we find that the inclusion of disorder effects in the theory is of qualitative importance, particularly at low carrier densities near the charge-neutral Dirac point (where the many-body effects are expected to be largest). The inclusion of disorder through two alternative physical approximations and the eventual validation of one of the models of disorder by comparing with the existing experimental data is an important accomplishment of our theory.

To outline the structure of this article, we begin in the remainder of this section by giving details of the band structures of the three types of graphene that we consider. In Sec. II we introduce a model for determining the band gap in bilayer graphene with arbitrary gate potentials applied to both layers. Then, in Sec. III we describe the calculation of $K = \frac{d\mu}{dn}$ in the homogeneous (nondisordered) situation (where μ and n are the chemical potential and carrier density, respectively) for each of these three cases, and discuss the main features of this quantity in relation to the quantum capacitance and compressibility. In Sec. IV we introduce the two models for the inclusion of disorder and present the fundamental theoretical results for each. Then, in Sec. V we compare the predictions of our theory to experimental data given by capacitance measurements of bilayer graphene, which include the quantum capacitance of the two-dimensional (2D) electron gas. Finally, in Sec. VI we summarize our results and give some general discussion of our findings.

In the following, we discuss three different models for the single-particle dispersion of graphene, which we denote by E_k . We shall refer to these three cases as linear, quadratic, and hyperbolic graphene to distinguish them. For the monolayer, we have $E_k^l = \hbar v_F k$, as is well known, and we indicate all quantities that follow from this dispersion by attaching a superscript l as we have here. For bilayer graphene, there are two commonly used approximations for the low-energy single-particle dispersion. The simplest is the quadratic approximation $E_k^q = \hbar^2 v_F^2 k^2 / \gamma_1 = \hbar^2 k^2 / (2m)$, where γ_1 is the interlayer hopping parameter from the tight-binding theory and $m = \gamma_1 / (2v_F^2)$ is the effective mass of the electrons. This dispersion comes from a low-energy effective theory of bilayer graphene,¹³ which essentially discards the two split bands and confines electrons to those lattice sites not involved in the interlayer coupling. This quadratic bilayer dispersion is assumed to hold for low carrier densities, i.e., at low Fermi energy.² Alternatively, the full tight-binding theory¹⁴ yields the single-particle dispersion,

$$E_k^h = \pm \sqrt{\frac{\gamma_1^2}{2} + \frac{u^2}{4} + \hbar^2 v_F^2 k^2} - \sqrt{\frac{\gamma_1^4}{4} + \hbar^2 v_F^2 k^2 (\gamma_1^2 + u^2)}, \quad (1)$$

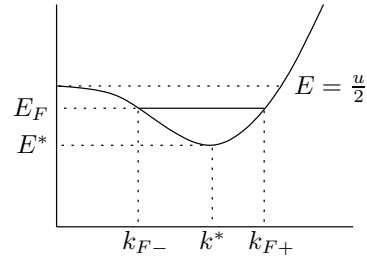


FIG. 1. Sketch of the “sombbrero” dispersion in hyperbolic graphene with $u > 0$. The depth of the minimum is exaggerated for purposes of illustration. The various wave vectors and energies that are labeled are defined in the text.

for the low-energy bands, which is illustrated for the conduction band in Fig. 1. This dispersion allows for the inclusion of a band gap parametrized by the energy u , which corresponds to the potential energy difference between the two layers. The “sombbrero” shape of the dispersion implies that the

minimum gap is found at wave vector $k^* = \frac{u}{2\hbar v_F} \sqrt{\frac{2\gamma_1^2 + u^2}{\gamma_1^2 + u^2}}$, and the energy of the minimum is therefore $E^* = \frac{\gamma_1 u}{2\sqrt{\gamma_1^2 + u^2}}$. This nonmonotonic dispersion relation leads to some important features in the Fermi surface at low density. For medium- and high-density regimes (when $k_F > \frac{u}{\hbar v_F}$), the Fermi wave vector is given by $k_F = \sqrt{\pi n}$ and the Fermi surface is disk shaped. However, if $\sqrt{\pi n} < \frac{u}{\hbar v_F}$ (as sketched in Fig. 1), then the Fermi energy is in the sombrero region and the Fermi surface is ring shaped¹⁵ with $k_{F-} < k < k_{F+}$ and

$$k_{F\pm} = \frac{1}{2\hbar v_F} \sqrt{\frac{\pi^2 \hbar^4 v_F^4 n^2 + \gamma_1^2 u^2}{\gamma_1^2 + u^2} + u^2 \pm 2\pi \hbar^2 v_F^2 n}. \quad (2)$$

Clearly these characteristic features of the full hyperbolic bilayer band dispersion are lost in the linear (“high-energy”) and quadratic (“low-energy”) approximations often adopted in the literature for simplicity.

The parameter u can be treated in two ways. Initially (and in Sec. IV), we consider it to be a phenomenological parameter that can be chosen arbitrarily to represent a finite gap at charge neutrality. However, in order to accurately compare our theory with experiment, we must determine a method of relating u to the external gate potentials. To do this accurately, the screening of the external field by the charge on the two layers of bilayer graphene must be taken into account, and we describe this process in Sec. II.

II. INTERLAYER SCREENING

In order to make an accurate comparison with experimental data, we must properly map the gate voltages applied in experiment to the parameters n and u that appear in our theory. We assume the situation sketched in Fig. 2(a). The density is easily computed via elementary considerations to be $n = \epsilon_0 (V_b \epsilon_b / d_b + V_t \epsilon_t / d_t) / e$, where V is the voltage applied to a gate, d is the width of the gate layer, ϵ is the dielectric constant of the gate, and the subscripts b and t respectively denote the bottom and top gates. The zeroth-order approximation for the on-site potential u is to say that the electric field created by

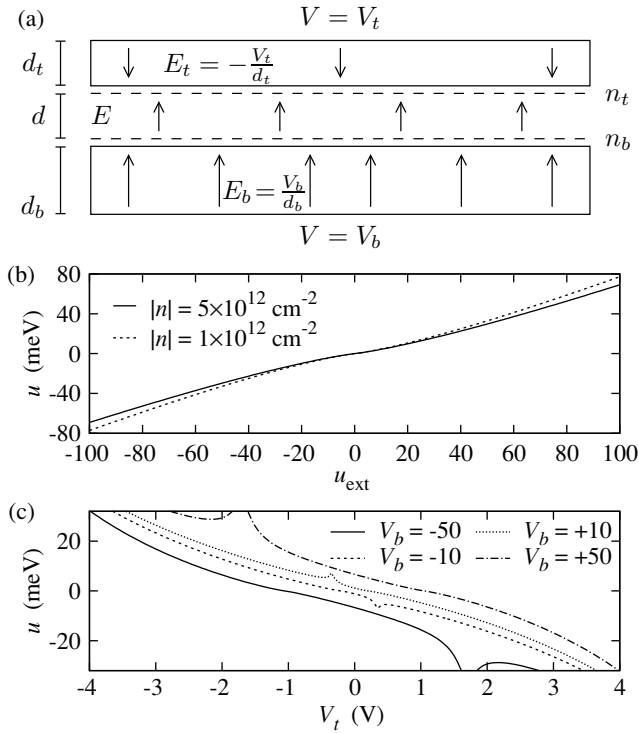


FIG. 2. (a) The geometry of the screening problem. The external field $E_{\text{ext}} = (E_b + E_t)/2$ is screened by redistribution of the charge density $n = n_b + n_t$ between the two layers of the graphene. (b) The screened gap u as a function of the bare gap u_{ext} for various densities. (c) The screened gap as a function of the top gate voltage for various fixed back gate voltages and the experimental parameters used in the experiments of Young *et al.* (Refs. 7 and 18). Back gate voltages are quoted in volts.

the gates directly gives the electric field E in the graphene. The potential is then $u_{t,b} = \pm eEd/2$. However, this approximation does not take into account the screening effect of the charge on the two graphene layers. Previously, various authors have investigated this problem and shown that screening reduces the size of the gap.^{14,16,17} We extend this work to the case where the total density is finite and gates are present both above and below the graphene layer.

Because the screening depends only on the electric field created by the gates and the charge densities on the two layers, it is independent of the disorder caused by charged impurities. Both the screening and the disorder effects are determined by the net carrier density, and both leave this quantity unchanged. Therefore, we can use the following analysis to set the size of the gap for any given set of external conditions, and use the resulting band structure to calculate the effect of disorder for that situation. This is allowed because neither disorder nor the screening induces any extra charge in the graphene. Additionally, we will assume in Sec. IV that the disorder potential is the same in both layers meaning that it does not induce any interlayer scattering and therefore leaves the net carrier density in each layer unchanged.

According to Gauss' law, the electric field directed away from an infinite-sized, positively charged sheet is $E = qn/2\epsilon_0$, where $q = -|e|$ is the charge of the carriers on the sheet.

Hence, we can write the internal field (i.e., the field between the graphene layers) as

$$E = E_{\text{ext}} + \frac{e}{2\epsilon_0}(n_t - n_b). \quad (3)$$

That the internal field is different from the external one causes the free charge on the two layers to rearrange, which in turn further modifies the internal field. A self-consistent procedure can be constructed to find the final solution for the layer charge densities and the internal electric field. This additional field causes an additional Hartree energy of $u_t - u_b = e d E$ to be added to the on-site potential in the original Hamiltonian. This modified on-site potential will be smaller than in the unscreened case, and therefore the gap will also be smaller.

We implement this procedure for a given pair of gate voltages V_b and V_t as follows. The first step is to compute the unscreened on-site potential in the two layers, which is given by the expression above with $n_t = n_b$ so that $E = E_{\text{ext}}$. This gives $u_{\text{ext}} = e d E_{\text{ext}} = e d (V_b/d_b - V_t/d_t)/2$. We assume that the potential is symmetrical so that $u_t = u/2$ and $u_b = -u/2$. This determines the single-particle Hamiltonian from which we can compute the wave functions. The layer density is then found by summing the wave-function weight in each layer:

$$n_t = \sum_{\text{states}} (|\phi_{At}|^2 + |\phi_{Bt}|^2),$$

where A and B label the two inequivalent lattice sites in each layer. The sum runs over all valley, spin, and wave-vector states. A similar expression is given for the lower layer by substituting $t \rightarrow b$ throughout. Computing these densities gives all the information required to evaluate the internal electric field, from which we can find the modified on-site potentials via Eq. (3). These potentials are then used to calculate the modified layer densities, and this cycle is repeated until convergence is reached.

Figure 2(b) shows the screened gap as a function of the external gap for various density of carriers. The density plays a role because the more free carriers there are, the more effectively the external field can be screened and the smaller is the screened gap. This is shown in the figure because the magnitude of the gap for $|n| = 5 \times 10^{12} \text{ cm}^{-2}$ is always smaller than that for $|n| = 1 \times 10^{12} \text{ cm}^{-2}$. Figure 2(c) shows the screened gap as a function of top gate voltage assuming that the back gate voltage is fixed. We have used the parameters from the experiments by Young *et al.*^{7,18} The peak in each trace is caused by the approach of the system to charge neutrality where there are no excess carriers and hence the external electric field is unscreened. At this point, the screened gap is equal to the bare gap. When there is a finite density of excess carriers, the external field is screened and the gap reduced accordingly. As the back gate voltage is changed, the position of the charge-neutrality point shifts and the size of the gap at charge neutrality increases. Inclusion of interlayer screening turns out to be important for understanding the experimental data.

III. CALCULATION OF $\frac{d\mu}{dn}$

In this section, we describe the calculation of $\frac{d\mu}{dn}$ for the homogeneous (nondisordered) system. The results derived

here will be used later to compute the same quantity for a disordered system. The single-particle dispersion E_k of monolayer and bilayer graphene are well known (as discussed in Sec. I). From these relations, we can compute the total kinetic energy for excess charge carriers by summing the energy of carriers in filled states, $\mathcal{E} = \sum_{\text{states}} E_k n_F(k)$, where $n_F(k)$ is the Fermi distribution function with wave vector $k = |\mathbf{k}|$. Then, the chemical potential is defined to be the change in energy with the addition of a particle, which is expressed as $\mu = \frac{1}{\mathcal{A}} \frac{d\mathcal{E}}{dn}$, where n is the carrier density and \mathcal{A} is the area of the graphene flake. From this we can compute $K = \frac{d\mu}{dn}$, and the quantum capacitance C_Q and compressibility κ are then linked to this quantity via

$$C_Q = \mathcal{A} e^2 \frac{dn}{d\mu}, \quad K^q = \frac{\hbar^2 v_F^2 \pi}{\gamma_1}. \quad (4)$$

The linear and quadratic band structures lead straightforwardly to the following expressions:

$$K^l = \frac{\hbar v_F \sqrt{\pi}}{2\sqrt{n}} \quad \text{and} \quad K^q = \frac{\hbar^2 v_F^2 \pi}{\gamma_1}.$$

The linear dispersion leads to a square-root divergence at zero density while the quadratic version gives a constant for all densities. It is possible to obtain an analytical expression for K^h in various limits, and we present them in the Appendix. Here, we describe a process for writing down the answer. Starting from the expression for the total energy, the sum is evaluated by transforming to an integral over k . The indefinite integral in question is given by

$$I(k) = \frac{2\mathcal{A}}{\pi} \int k E_k^h dk. \quad (5)$$

To find the total energy, we write the sum over states discussed above as an integral over the wave vector. Then, evaluation of the Fermi function naturally leads to an expression containing $I(k)$ at the limiting values of the wave vector for the specific value of the density:

$$\mathcal{E} = \frac{2\mathcal{A}}{\pi} \int_0^\infty k E_k^h n_F(k) dk = I(k = k_{F+}) - I(k = k_{F-}).$$

The chemical potential can be calculated by transforming the derivative into one for the limiting k :

$$\mu = \frac{1}{\mathcal{A}} \frac{d\mathcal{E}}{dn} = \frac{1}{\mathcal{A}} \frac{dk_{F+}}{dn} \frac{dI(k_{F+})}{dk_{F+}} - \frac{1}{\mathcal{A}} \frac{dk_{F-}}{dn} \frac{dI(k_{F-})}{dk_{F-}}.$$

However, it is clear from the fundamental theorem of calculus and the definition of I that $dI/dk = 2\mathcal{A}kE_k/\pi$ so that the second derivative is straightforward to calculate, and we have

$$\begin{aligned} K^h = \frac{2}{\pi} & \left[\frac{d^2 k_{F+}}{dn^2} k_{F+} E_{k_{F+}} - \frac{d^2 k_{F-}}{dn^2} k_{F-} E_{k_{F-}} \right. \\ & + \left(\frac{dk_{F+}}{dn} \right)^2 \left(E_{k_{F+}} + k_{F+} \frac{dE_{k_{F+}}}{dk_{F+}} \right) \\ & \left. - \left(\frac{dk_{F-}}{dn} \right)^2 \left(E_{k_{F-}} + k_{F-} \frac{dE_{k_{F-}}}{dk_{F-}} \right) \right]. \end{aligned} \quad (6)$$

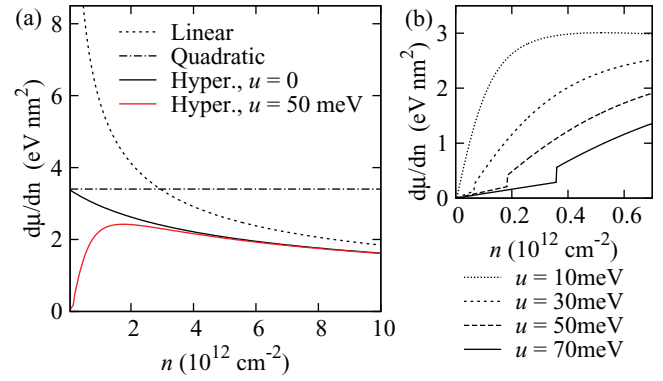


FIG. 3. (Color online) (a) The inverse density of states, $K = \frac{d\mu}{dn}$, for linear, quadratic, gapless hyperbolic, and gapped hyperbolic ($u = 50 \text{ meV}$) dispersions. (b) K for different gap sizes at low carrier density.

The remaining derivatives are simple to compute from Eqs. (1) and (2). As described previously, when $|E_F| < u/2$, the values of k_{\pm} are given by Eq. (2). When $|E_F| > u/2$ (which is trivially the case for $u = 0$) then $k_- = 0$ and $k_+ = \sqrt{\pi n}$ and only the first two terms contribute to K^h . This is the central result of this section, but in the Appendix we have evaluated this expression for various limiting cases.

The three versions of K are plotted in Fig. 3(a) where the density is assumed to be a tunable external parameter and the gap is fixed. In the limit of small n , the gapless hyperbolic band structure is roughly quadratic and so K^h is very close to K^q . However, the linearity of the hyperbolic dispersion quickly asserts itself to reduce the size of K^h until, at high density, it approaches the value of linear graphene. Thus K^h in the ungapped regime interpolates between these two limiting cases, as one expects. We also show K^h for the gapped case (red or light gray line) where we take $u = 50 \text{ meV}$. When the density is high and the Fermi energy is well above the gap region, K^h tends to the same functional form as for the ungapped scenario. However, when the density is low, K^h goes to zero for any finite u . The large reduction in K^h by the gap will be an important feature for the comparison with experiment. In Fig. 3(b) we show the K^h at low carrier density for several different values of the gap. One immediately notices a discontinuity when $n = u/(\hbar v_F)$, which is caused by the change in topology of the Fermi surface from a ring to a disk. When a gap is present, there is also a δ -function divergence at $n = 0$ (not shown in the plots) caused by the step in the chemical potential as the Fermi energy goes from the valence band to the conduction band. The prefactor of this divergence is the size of the gap so that it is not present when $u = 0$.

IV. MODELS FOR DISORDER

We now discuss the effects of disorder caused by electron-hole puddles that are formed by charged impurities in the environment.^{5,19} We will describe two inequivalent methods of averaging over disorder and highlight the differences between them. In what follows, we must be careful to distinguish global (averaged) quantities from their local counterparts. Therefore, we use an overbar to denote a quantity that has been averaged over disorder and that is therefore global. We start by assuming

that charged impurities (which may be located in the substrate or near the graphene) create a local electrostatic potential that fluctuates randomly across the surface of the graphene sheet. In the case of the bilayer, we assume that this potential is felt equally by both layers. We then make the transition from the spatial variation of the potential to an average by assuming that the value of this potential at any given point can be described by a statistical distribution.²⁰ This distribution can then be used to average some pertinent quantity to obtain the bulk result for the disordered system. But it is not clear *a priori* what the optimum method of performing this average is. In order to discuss this question, we use two different methods and (in the next section) compare the results of each to experimental data.

The first model assumes that the disorder potential directly affects the density of carriers in the graphene so that the density is distributed according to a Gaussian distribution P parametrized by width v ,

$$P(n) = \frac{1}{v\sqrt{2\pi}} \exp\left(-\frac{n^2}{2v^2}\right).$$

Then, the overall value of $\bar{K} = \frac{d\mu}{dn}$ can be found by evaluating the convolution of the homogeneous (nondisordered) K with this distribution:

$$\frac{d\mu}{dn} = \int_{-\infty}^{\infty} \frac{d\mu(n-n')}{d(n-n')} P(n') dn'. \quad (7)$$

This has the effect of broadening any sharp features in the homogenous K , such as the δ function at $n = 0$ in a gapped system or the step associated with the change in topology of the Fermi surface in the hyperbolic band. Specifically, evaluating this convolution gives the following contribution to \bar{K} for the hyperbolic band from the δ function,

$$\frac{u\gamma_1}{\sqrt{u^2 + \gamma_1^2}} \frac{\exp[-n^2/2(\delta n)^2]}{\delta n\sqrt{2\pi}},$$

so that this spike is broadened into a peak where the height is determined by the size of the effective gap $2E^*$. This model corresponds to that taken in Ref. 8, except that our theory includes the interlayer screening, which reduces the gap size.

The second model assumes that the disorder potential introduces variation in the density of states (DOS). The potential itself is assumed to follow a Gaussian distribution $P(V)$ parametrized by width s , and therefore the disordered

DOS is given by²⁰

$$D(E) = \int_{-\infty}^{\infty} D_0(E-V)P(V)dV, \quad (8)$$

where $D_0(E)$ is the homogeneous (nondisordered) DOS. This modified DOS then gives the zero-temperature electron density by integrating over energy so that

$$\bar{n}(E_F) = \int_{-\infty}^{\infty} D(E)\Theta(E_F - E)dE, \quad (9)$$

where E_F is the global Fermi energy and $\Theta(x)$ is the Heaviside step function. A similar expression exists for the density of holes. This density is assumed to hold throughout the graphene so that the averaged density can now be used to evaluate $\bar{K} = \frac{d\mu(\bar{n})}{dn}$. Because we assume that the disorder does not induce any additional charge in the 2D system, the net carrier density $n^e - n^h$ is conserved. Therefore, to compute the effective Fermi energy \bar{E}_F in the presence of disorder, we solve the equation $\bar{n}^e(\bar{E}_F) - \bar{n}^h(\bar{E}_F) = n_0^e(E_F) - n_0^h(E_F)$ for \bar{E}_F . However, the total carrier density $n^e + n^h$ is not conserved, and the primary effect of disorder in this model is to introduce a finite total density for any finite amount of charged impurities.

The integrals in Eqs. (8) and (9) can be computed analytically for the linear and quadratic bands if we assume that $P(V)$ is a Gaussian distribution. They are

$$\bar{n}^l = \frac{1}{\pi\hbar^2 v_F^2} \left[\frac{E_F^2 + s^2}{2} \text{erfc}(\mp y) \pm \frac{E_F s}{\sqrt{2\pi}} e^{-y^2} \right]$$

and

$$\bar{n}^q = \frac{\gamma_1}{2\pi\hbar^2 v_F^2} \left[s\sqrt{\frac{2}{\pi}} e^{-y^2} \pm E_F \text{erfc}(\mp y) \right],$$

where the upper sign corresponds to the electron density and the lower sign to the hole density, erfc is the complementary error function, and $y = E_F/(\sqrt{2}s)$, with s the standard deviation of the distribution of the disorder potential. We see that the effect of disorder is to introduce a tail in the electron density that extends into the conduction band, the size of which increases with increasing disorder strength. In the hyperbolic case, the integrals in Eqs. (8) and (9) cannot be evaluated analytically, so a numerical comparison must be done with the other two cases.

The expressions that must be computed for the hyperbolic band are

$$n^{he} = \frac{1}{s\sqrt{2\pi}} \frac{1}{\pi\hbar^2 v_F^2} \int_{-\infty}^{E_F} dE \left[\int_{-\infty}^{E-E^*} dV(E-V)[2 + \mathcal{F}(E-V)]e^{-V^2/(2s^2)} - \int_{E-\frac{u}{2}}^{E-E^*} dV(E-V)[2 - \mathcal{F}(E-V)]e^{-V^2/(2s^2)} \right]$$

and

$$n^{hh} = \frac{1}{s\sqrt{2\pi}} \frac{1}{\pi\hbar^2 v_F^2} \int_{E_F}^{\infty} dE \left[- \int_{E+E^*}^{\infty} dV(E-V)[2 + \mathcal{F}(E-V)]e^{-V^2/(2s^2)} + \int_{E+E^*}^{E+\frac{u}{2}} dV(E-V)[2 - \mathcal{F}(E-V)]e^{-V^2/(2s^2)} \right],$$

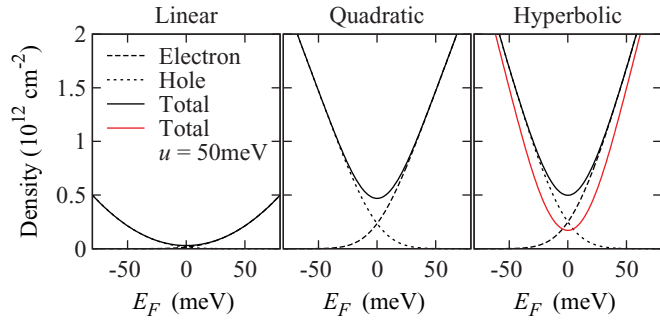


FIG. 4. (Color online) Electron, hole, and total carrier densities for linear, quadratic, and hyperbolic graphene for $s = 20$ meV.

where $\Delta = 1 + u^2/\gamma_1^2$, $\mathcal{F}(x) = \Delta/\sqrt{\Delta x^2/\gamma_1^2 - \delta^2}$, and in both cases the second term comes from the inner Fermi surface for $E^* < |E| < u/2$.

Figure 4 shows the density of carriers in these three cases for a modest value of disorder ($s = 20$ meV) and also for $u = 50$ meV in hyperbolic graphene. The small density of states in linear graphene gives a small carrier density at low Fermi energy. Quadratic and hyperbolic graphene have finite DOS at charge neutrality so the density is higher in this case. The density in hyperbolic graphene increases slightly quicker than quadratic graphene because of the linear increase in the DOS compared to the constant density of states in quadratic graphene. Also, the finite density of states at the charge-neutrality point in quadratic and hyperbolic graphene means that the effect of disorder is significantly stronger in these systems than in linear graphene. In fact, substituting $E_F = 0$ into the total density gives the dependence of the density at the charge-neutrality point as a function of the disorder strength s as

$$\bar{n}^l(E_F = 0) = \frac{s^2}{\pi \hbar^2 v_F^2}, \quad \bar{n}^q(E_F = 0) = \sqrt{\frac{2}{\pi}} \frac{\gamma_1 s}{\pi \hbar^2 v_F^2},$$

so that the linear increase in $\bar{n}^q(E_F = 0)$ is faster than the quadratic one in $\bar{n}^l(E_F = 0)$ for small s . The density at charge neutrality in hyperbolic graphene is identical to that in quadratic graphene because the DOS is the same in both cases. We emphasize that both models of disorder considered here are physically motivated and *a priori* there does not appear to be any practical reason to choose one over the other. In the next section, we compare theory with recent graphene compressibility experimental data to establish the comparative validity of our disorder models.

V. EXPERIMENTAL COMPARISON: THE EFFECT OF DISORDER

We now discuss our results in the context of recently published experiments. We restrict ourselves to comparison with the bilayer because it is known that the effect of disorder in monolayer graphene is small, and this has already been discussed in the literature.⁶ In particular, two measurements have been reported where the capacitance of bilayer graphene has been measured and the compressibility extracted from those measurements.^{7,8} The quantum capacitance is linked to $\frac{d\mu}{dn}$ because $C_Q = \mathcal{A}e^2 \frac{dn}{d\mu}$, where \mathcal{A} is the surface area of

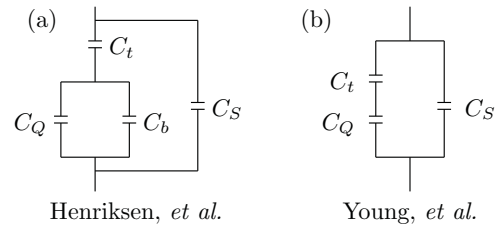


FIG. 5. Classical circuit diagrams for the experiments by (a) Henriksen *et al.* (Ref. 8) and (b) Young *et al.* (Ref. 7).

the sample. The two experiments actually measure slightly different capacitances, which are represented by the two circuit diagrams in Fig. 5 and correspond to the following expressions for the measured capacitances C_H and C_Y :

$$C_Y = \frac{\mathcal{A}\epsilon_0\epsilon_t}{\epsilon_t d_g + d_t} + C_S, \quad \text{Young (Ref. 7)}$$

$$C_H = \frac{\epsilon_0\epsilon_b\epsilon_t d_g \mathcal{A}}{d_g(\epsilon_b d_t + \epsilon_t d_b) + d_b d_t} + C_S, \quad \text{Henriksen (Ref. 8).}$$

The notation follows that defined in Fig. 2(a), except that d_g is an effective length associated with the quantum capacitance as

$$C_Q = \frac{\mathcal{A}\epsilon_0}{d_g} \Rightarrow d_g = \frac{\epsilon_0}{e^2} \frac{d\mu}{dn}.$$

The quantity C_S is the background (or stray) capacitance associated with, for example, the substrate and experimental equipment. For relevant experimental parameters, $d_g \ll d_b, d_t$ so that $C_H \propto d_g \propto \frac{d\mu}{dn}$. We find the relevant experimental parameters from the papers¹⁸ and use them to produce the plots shown in Figs. 6 and 7. Note that if the quadratic band structure is used to compute C_H and C_Y , so that $d_g = \hbar^2 v_F^2 \epsilon_0 \pi / (e^2 \gamma_1)$, then there is no density dependence in either C_H or C_Y , which is qualitatively different to the experimental data in Figs. 6 and 7. Therefore, the full band structure is an essential part of our theory.

Figure 6 shows the comparison of data from both disorder models to the experiments⁷ of Young *et al.* In this case, the back gate is kept at a fixed potential while the top gate is varied. This has the effect of simultaneously changing the size of the gap and the carrier density so in this case we treat these two quantities separately and use the full theory of the interlayer screening described in Sec. II to compute the size of the effective gap. When the gap is small at low density [i.e., for $V_b = 10$ V, Fig. 6(a)] both theories of disorder predict qualitatively correct answers. The difference between the experimental and theoretical curves can be reduced by changing the value of the stray capacitance as a fitting parameter. For very low values of disorder, a small spike is present at zero density in the density-averaged data. This is owing to the very small band gap that is present and the associated δ function in $\frac{d\mu}{dn}$. Larger values of disorder smear this divergence out into a dip, the shape of which matches the experimental data well. The DOS-averaged plots do not show this dip because carrier density is always finite in this model, and the effect of increasing disorder is to increase the minimum value of the carrier density, thus decreasing the depth of the dip. When the gap is large at zero density [i.e., for large back gate voltage, $V_b = 70$ V, Fig. 6(b), and $V_b = -80$ V, Fig. 6(c)], then the

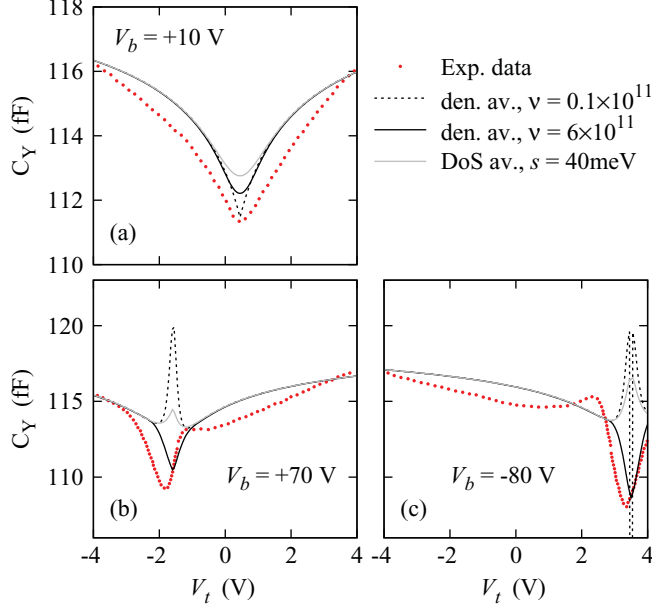


FIG. 6. (Color online) Comparison of theoretical results including disorder for the measured capacitance C_Y with experimental data by Young *et al.* (Ref. 7). We have taken $\gamma_1 = 0.35$ eV and $v_F = 1.05 \times 10^6$ ms $^{-1}$.

DOS-averaging procedure predicts qualitatively wrong results for low values of disorder. There are two main features in the low-density part of these plots. First, for finite gap, Fig. 3 shows that $\frac{d\mu}{dn}$ tends to zero as density decreases. This gives a peak in the measured capacitance [because $C_Y \propto 1/(\frac{d\mu}{dn} + \frac{e^2 d_t}{\epsilon_0 \epsilon_r})$], which is blurred by finite disorder. The second feature is the δ function at the band edge (or, equivalently, at zero density), which is broadened by finite disorder in the density-averaging model, but which plays no role in the DOS-averaging model because this model always gives rise to a finite density of carriers. This means that the DOS average cannot predict correct results in the low-density, finite-gap regime. However, the density-averaging model does include the effects of the δ -function spike by sampling many values of density, and crucially including $n = 0$. This spike in $\frac{d\mu}{dn}$ manifests as the dip in the measured capacitance, and parameters can be chosen so that the size and shape of the dip match the experimental data quite closely. We therefore believe the density-averaging procedure of Eq. (7) to be the preferable model for including disorder over the the DOS-averaging model.

This general picture is also seen in the comparison of the two disorder theories with data by Henriksen *et al.* as shown in Fig. 7. Figures 7(c) and 7(d) show the comparison of the experimental data to the DOS-averaged model. In this experiment, the measured capacitance is proportional to $\frac{d\mu}{dn}$, so in the gapped case in Fig. 7(d), the step in $\frac{d\mu}{dn}$ owing to the change in topology of the Fermi surface is clearly seen for large gap. The zero-gap data in Fig. 7(c) shows qualitatively the correct features, although the stray capacitance must be altered to get a better fit and the peak is taller in the experimental data than in the theory. But when the gap is opened as shown in Fig. 7(d), the DOS-averaged theory predicts qualitatively wrong results because it does not account for the broadened

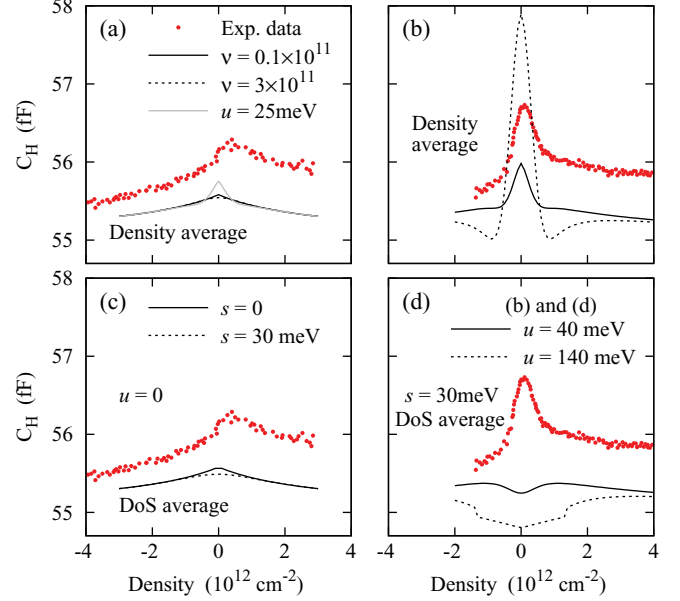


FIG. 7. (Color online) Comparison of theoretical results including disorder with experimental data by Henriksen *et al.* (Ref. 8). (a) $u_{\text{ext}} = 0$ compared with the density-averaged model for zero gap and a small gap, and $u = 25$ meV for $\nu = 3 \times 10^{11}$ cm $^{-2}$. (b) u_{ext} finite, compared with the density-averaged theory for several values of the gap. We have taken $\nu = 3 \times 10^{11}$ cm $^{-2}$ and the legend is as shown in (d). (c) DOS-averaged theory compared with $u_{\text{ext}} = 0$ experimental data for $s = 0$ and $s = 30$ meV. (d) u_{ext} finite compared with DOS-averaged theory for two values of the gap. $s = 30$ meV in each case. We have taken $\gamma_1 = 0.35$ eV and $v_F = 1.05 \times 10^6$ ms $^{-1}$ throughout.

δ function associated with the band edges. The experimental data also shows a distinct asymmetry between the electron- and hole-density regimes. This is not explained in our model, but can be added by allowing for an asymmetry in the underlying band structure, for example by including specific next-nearest-neighbor hops in the tight-binding model.²¹ On the other hand, the density-averaging theory [shown in Figs. 7(a) and 7(b)] do predict the correct behavior. For the zero-gap experiment, the variation of the predicted C_H is too small, and better agreement can be found by allowing for a small gap to open, as shown by the dashed line. In Fig. 7(b), it is clear that a gap size of ≈ 40 meV gives a semiquantitative fit to the experiment.

VI. CONCLUSION AND DISCUSSION

In conclusion, we have presented a full calculation of $\frac{d\mu}{dn}$ (and hence the quantum capacitance and compressibility) for graphene and have discussed two different methods for including disorder effects. These models require averaging the effect of the disorder potential in either the DOS or directly as a variation in the local electron density. We find that when there is no gap in the system, these two models predict qualitatively similar results. But when there is a gap present, the DOS-averaging method fails to account for the step in the chemical potential owing to the band edges and therefore predicts qualitatively incorrect results. So, we present two conclusions: First, that the single-particle theory for the compressibility of graphenes appears to allow qualitatively

good predictions for thermodynamic quantities such as the compressibility. Second, the inclusion of disorder via statistical averaging must be done carefully because the choice of where the averaging is done critically affects the outcome. We find that the averaging should be carried out at the level of the experimental quantity rather than the DOS.

We believe that the effects left out of the theory, particularly the many-body exchange-correlation corrections, are likely to be qualitatively unimportant for understanding the experimental data for currently available graphene samples that are dominated by disorder. In particular, disorder effects are strongest at the lowest carrier densities where exchange-correlation effects become more important quantitatively. This makes an observation of many-body effects through compressibility measurements quite challenging.

ACKNOWLEDGMENTS

We thank J. P. Eisenstein, E. A. Henriksen, P. Kim, and A. Young for discussions of their experimental results. This work was supported by US-ONR and NRI-SWAN.

APPENDIX: ANALYTICAL RESULTS FOR K^h

In this Appendix, we give the derivation of K^h , and write down the full expression for it in various cases. The full form of the indefinite integral in Eq. (5) is

$$\begin{aligned} I(k) &= \frac{2\mathcal{A}}{\pi} \int k E_k^h dk \\ &= \frac{\mathcal{A}\gamma_1^3}{\pi\hbar^2 v_F^2} \frac{1}{24\sqrt{\Delta}} \{ \sqrt{2\Delta}(8x - \Phi + 1 - 4\delta^2)\Xi \\ &\quad + 12\delta^2 \log[2\Delta(-\Delta + \Phi + \sqrt{2\Delta}\Xi)] \}, \end{aligned}$$

where $x = (\hbar v_F k / \gamma_1)^2$, $\delta = u/(2\gamma_1)$, $\Phi = \sqrt{1 + 4x\Delta}$, $\Xi = \sqrt{2x - \Phi + 1 + 2\delta}$, and $\Delta = 1 + 4\delta^2$. Explicitly differentiating with respect to k verifies the fundamental theorem of calculus, which we utilized in the description of Eq. (6). In the general case, the derivative of the energy with respect to the wave vector is

$$\frac{dE_{k_F}^h}{dk_F} = \frac{\hbar^2 v_F^2 k_F}{E_{k_F}^h} \left(1 - \frac{\gamma_1^2 + u^2}{2\sqrt{\frac{\gamma_1^4}{4} + \hbar^2 v_F^2 k_F^2 (\gamma_1^2 + u^2)}} \right). \quad (\text{A1})$$

1. The $u = 0$ limit

In this case, $k_F = \sqrt{\pi n}$ for all densities. Therefore, the derivatives of k_F with respect to n are elementary, the $k_{F\pm}$ terms in Eq. (6) trivially do not contribute, and we have

$$K_{u=0}^h = \frac{\gamma_1}{n_0 \sqrt{\frac{1}{2} + \frac{n}{n_0} - \sqrt{\frac{1}{4} + \frac{n}{n_0}}}} \left(\frac{1}{2} - \frac{1}{4\sqrt{\frac{1}{4} + \frac{n}{n_0}}} \right),$$

where $n_0 = \gamma_1^2 / (\pi \hbar^2 v_F^2)$.

2. When $u > 0$, $|E_F| > u/2$

When $|E_F| > u/2$, then $k_{F+} = \sqrt{\pi n}$ and $k_{F-} = 0$ so that the derivatives with respect to n are elementary and only the first two terms of Eq. (6) contribute to K^h . Therefore,

$$\begin{aligned} K^h(|E_F| > u/2) &= \frac{\gamma_1}{2n_0 \sqrt{\frac{1}{2} + \frac{n}{n_0} + \frac{u^2}{4} - \sqrt{\frac{1}{4} + \frac{n}{n_0} \frac{n_{0u}}{n_0}}}} \left(1 - \frac{n_{0u}/n_0}{2\sqrt{\frac{1}{4} + \frac{n}{n_0} \frac{n_{0u}}{n_0}}} \right). \end{aligned}$$

3. When $u > 0$, $|E_F| < u/2$

However, when $|E_F| < u/2$, we need to use the expressions for the two Fermi surfaces in Eq. (2) so that

$$\frac{dk_{F\pm}}{dn} = \frac{\pi}{4k_{F\pm}} \left(\frac{n}{n_{0u}} \pm 1 \right),$$

where $n_{0u} = (\gamma_1^2 + u^2) / (\pi \hbar^2 v_F^2)$ and hence

$$\frac{d^2 k_{F\pm}}{dn^2} = \frac{\pi}{4k_{F\pm}} \left[\frac{1}{n_{0u}} - \frac{\pi}{4k_{F\pm}^2} \left(\frac{n}{n_{0u}} \pm 1 \right)^2 \right].$$

Substituting these expressions for the derivatives into Eq. (6) gives the simplified expression

$$\begin{aligned} K^h(|E_F| < u/2) &= \frac{\pi}{8} \left[\frac{1}{k_{F+}} \left(\frac{n}{n_{0u}} + 1 \right)^2 \frac{dE_{k_{F+}}}{dk_{F+}} \right. \\ &\quad \left. - \frac{1}{k_{F-}} \left(\frac{n}{n_{0u}} - 1 \right)^2 \frac{dE_{k_{F-}}}{dk_{F-}} \right], \end{aligned}$$

where the derivatives of the Fermi energy with respect to the Fermi wave vector are given by making the appropriate substitutions in Eq. (A1).

¹D. S. L. Abergel, V. Apalkov, J. Berashevich, K. Ziegler, and T. Chakraborty, *Adv. Phys.* **59**, 261 (2010).

²S. Das Sarma, S. Adam, E. H. Hwang, and E. Rossi, *Rev. Mod. Phys.* (in press).

³D. L. John, L. C. Castro, and D. L. Pulfrey, *J. Appl. Phys.* **96**, 5180 (2004).

⁴T. Fang, A. Konar, H. Xing, and D. Jena, *Appl. Phys. Lett.* **91**, 092109 (2007).

⁵J. Martin, N. Akerman, G. Ulbricht, T. Lohmann, J. H. Smet, K. von Klitzing, and A. Yacoby, *Nat. Phys.* **4**, 144 (2008).

⁶E. H. Hwang, B. Y.-K. Hu, and S. Das Sarma, *Phys. Rev. Lett.* **99**, 226801 (2007).

⁷A. F. Young, C. R. Dean, I. Meric, S. Sorgenfrei, H. Ren, K. Watanabe, T. Taniguchi, J. Hone, K. L. Shepard, and P. Kim, e-print [arXiv:1004.5556v2](https://arxiv.org/abs/1004.5556v2).

⁸E. A. Henriksen and J. P. Eisenstein, *Phys. Rev. B* **82**, 041412(R) (2010).

⁹J. Xia, F. Chen, J. Li, and N. Tao, *Nat. Nano.* **4**, 505 (2009). See supplementary information for experimental data relating to bilayer graphene.

- ¹⁰S. V. Kusminskiy, J. Nilsson, D. K. Campbell, and A. H. Castro Neto, *Phys. Rev. Lett.* **100**, 106805 (2008).
- ¹¹G. Borghi, M. Polini, R. Asgari, and A. H. MacDonald, *Phys. Rev. B* **82**, 155403 (2010).
- ¹²R. Sensarma, E. H. Hwang, and S. Das Sarma, e-print [arXiv:1102.1427](https://arxiv.org/abs/1102.1427) (unpublished).
- ¹³E. McCann and V. I. Fal'ko, *Phys. Rev. Lett.* **96**, 086805 (2006).
- ¹⁴E. McCann, *Phys. Rev. B* **74**, 161403(R) (2006).
- ¹⁵T. Stauber, N. M. R. Peres, F. Guinea, and A. H. Castro Neto, *Phys. Rev. B* **75**, 115425 (2007).
- ¹⁶H. Min, B. Sahu, S. K. Banerjee, and A. H. MacDonald, *Phys. Rev. B* **75**, 155115 (2007).
- ¹⁷E. V. Castro, K. S. Novoselov, S. V. Morozov, N. M. R. Peres, J. M. B. Lopes dos Santos, J. Nilsson, F. Guinea, A. K. Geim, and A. H. Castro Neto, *Phys. Rev. Lett.* **99**, 216802 (2007).
- ¹⁸We find for the experiments of Young *et al.* that $\epsilon_t = 2.3$, $\epsilon_b = 3.7$, $d_t = 6$ nm, $d_b = 285$ nm, $A = 31 \mu\text{m}^2$, and $C_S = 15$ fF. For the data of Henriksen *et al.* we have $\epsilon_t = 3.3$, $\epsilon_b = 3.9$, $d_t = 27$ nm, $d_b = 310$ nm, $A = 250 \mu\text{m}^2$, and $C_S = 54.8$ fF.
- ¹⁹E. Rossi and S. Das Sarma, *Phys. Rev. Lett.* **101**, 166803 (2008); S. Das Sarma, E. H. Hwang, and E. Rossi, *Phys. Rev. B* **81**, 161407 (2010).
- ²⁰E. H. Hwang and S. Das Sarma, *Phys. Rev. B* **82**, 081409 (2010).
- ²¹Z. Q. Li, E. A. Henriksen, Z. Jiang, Z. Hao, M. C. Martin, P. Kim, H. L. Stormer, and D. N. Basov, *Phys. Rev. Lett.* **102**, 037403 (2009); A. B. Kuzmenko, I. Crassee, D. van der Marel, P. Blake, and K. S. Novoselov, *Phys. Rev. B* **80**, 165406 (2009).